CHALMERS | UNIVERSITY OF GOTHENBURG

PREPRINT 2009:34

Globally Convergent Numerical Methods for Coefficient Inverse Problems for Imaging Inhomogeneities

JIANGUO XIN
LARISA BEILINA
MICHAEL V. KLIBANOV

Department of Mathematical Sciences
Division of Mathematics
CHALMERS UNIVERSITY OF TECHNOLOGY
UNIVERSITY OF GOTHENBURG
Göteborg Sweden 2009

Preprint 2009:34

Globally Convergent Numerical for Coefficient Inverse Problems for Imaging Inhomogeneities

Jianguo Xin, Larisa Beilina, Michael V. Klibanov

Department of Mathematical Sciences
Division of Mathematics
Chalmers University of Technology and University of Gothenburg
SE-412 96 Göteborg, Sweden
Göteborg, August 2009

Preprint 2009:34
ISSN 1652-9715

Matematiska vetenskaper
Göteborg 2009

Globally Convergent Numerical Methods for Coefficient Inverse Problems for Imaging Inhomogeneities

Jianguo Xin*, Larisa Beilina† and Michael V. Klibanov*

Abstract

How can we differentiate between an underground stone and a land mine? We discuss a class of methods for solving such problems. This class of methods concerns globally convergent numerical methods for Coefficient Inverse Problems, unlike conventional locally convergent algorithms. Numerical results are presented modeling imaging of the spatially distributed dielectric permittivity function in an environment where antipersonnel land mines are embedded along with stones. While these results are concerned with the first generation of globally convergent algorithms, images obtained by the most recent second generation are also presented for a generic case of imaging of the dielectric permittivity function. The mathematical apparatus is sketched only very briefly with references to corresponding publications.

1 Introduction

The goal of this publication is to present to the engineering community a new development in numerical methods for the so-called Coefficient Inverse Problems for Partial Differential Equations (PDEs). All necessary mathematical details can be found in [6, 4, 5, 27, 28, 43, 44, 45, 46], so we provide only a minimum of such details here. Convergence of the new algorithms to the correct solution does not depend on the availability of a proper first guess of the solution. This is both rigorously guaranteed and numerically confirmed. While works [27, 28, 43, 44, 45, 46] on the so-called 'convexification' algorithm represent the first generation of globally convergent numerical methods, in publications [6, 4, 5] the second generation of these numerical methods has started.

These new techniques are most suitable for imaging of small abnormalities embedded in otherwise slowly varying and unknown background. 'Imaging' means locating those small abnormalities and obtaining accurate estimates of their features. Conventional numerical methods for Coefficient Inverse Problems are based on the small perturbation approach and converge locally; i.e. they need a good first guess for the solution, and the solution they find is a small perturbation of this initial guess. While locally convergent numerical methods usually locate abnormalities well enough, they can rather rarely estimate values of unknown coefficients within abnormalities accurately. Accurate estimates potentially enable

*Department of Mathematics and Statistics, University of North Carolina at Charlotte, Charlotte, NC 28223-0001, USA. E-mail address: {jxin;mklibanv}@uncc.edu.

†Department of Mathematical Sciences, Chalmers University of Technology and Gothenburg University, Gothenburg, SE-42196, Sweden. E-mail address: larisa.beilina@chalmers.se

one to identify abnormalities, e.g. to differentiate between land mines and stones or between malignant and benign abnormalities in human organs.

Imaging of small abnormalities is important in many applications. Some examples are in imaging of the dielectric permittivity function within antipersonnel land mines, imaging of tumors in human organs, imaging of acoustic abnormalities in underwater, etc. We provide some numerical examples for the case of land mines as well as for a generic case. For example, we show that our first generation numerical method can differentiate between a land mine and a stone (within the framework of our mathematical model).

2 Inverse and Ill-posed Problems

Inverse problems arise in quite many fields of science and engineering, for example, in medical imaging, image and signal processing, mathematical finance, astronomy, geophysics, remote sensing, radar imaging, ocean acoustic tomography, nondestructive material testing and subsurface prospecting, etc. Solution of inverse problems requires determining unknown features (parameters) based on observations (data) of their effects. This is in contrast to the classic *direct problems*, whose solution involves finding effects based on complete descriptions of their causes. Direct problems for PDEs are described in many textbooks, see, e.g. [16]. "Can one hear the shape of a drum?" is a famous inverse problem which was posed by the noted mathematician Mark Kac [22]. Literally, if you have perfect pitch, can you find the shape of a drum? Mathematically this asks whether a plane region R can be determined from the natural frequencies of a membrane fixed along the edge of R.

Inverse problems are inherently ill-posed, as opposed to well-posed direct problems. The mathematical term well-posed problem was defined by the renowned mathematician Jacques Hadamard [19], who believed that mathematical models of physical phenomena should have the following three properties:

- A solution exists (existence),
- The solution is unique (uniqueness),
- The solution depends continuously on the given data in a certain reasonable topology (stability).

Thus a problem is well-posed if a unique solution exists and depends continuously on the data. Of the three conditions for a well-posed problem the condition of stability is most often violated. Ill-posed problems may arise because of the unavailability of some boundary data. Or, they may crop up due to the lack of information of the location of internal cracks, heterogeneities or singularities. Or, they may appear since we do not simply have the necessary data [33].

Classification of inverse problems is rather arbitrary. One approach of sorting them is by the type of information that is being sought in the solution procedure. In particular, we are interested in the so-called Coefficient Inverse Problems which belong, in a broader sense, to

the category of the classic parameter estimation problems where an unknown coefficient in a governing PDE is to be found. In a Coefficient Inverse Problem one is supposed to determine an unknown spatially distributed coefficient of a PDE from boundary measurements of the solution of this PDE. Coefficient Inverse Problems are of tremendous practical importance. The coefficient to be found has direct physical meaning and is usually associated with the characteristics of the media under consideration [21]. Recovery of the Lamé parameter in biological tissues [20], reconstruction of the conductivity coefficient in electrical impedance tomography [12], and shear wave speed recovery in transient elastography [31] are some concrete examples of coefficient inverse problems.

To obtain a stable numerical method for an inverse problem, a technique called regularization is usually needed to introduce mild assumptions on the solution. The classic Tikhonov regularization [38, 39] is the most popular one, whose key idea is a trade-off between fitting the data and reducing a norm of the solution. There are several ramifications based upon the idea of Tikhonov regularization and of particular interest is the quasi-reversibility method [30, 13, 8, 10]. The key idea of the quasi-reversibility method is that one changes the originally ill-posed problem into a properly-posed problem by perturbing the governing equations and perhaps the boundary conditions as well. Then based on the solution of the perturbed problem one obtains an approximate solution of the formerly ill-posed problem. The appropriate perturbation to the governing equations of the ill-posed problem is usually not unique. Depending upon how one determines this, the solution process of constructing an approximate solution of the ill-posed problem may be quite different [25]. The quasi-reversibility method shares the same spirit as the method of artificial viscosity in computational fluid dynamics. There one adds a viscosity term to the governing equations to stabilize the problem and then studies the asymptotic behavior of the solution as the perturbation goes to zero [42].

3 Background

Researchers in the field of Coefficient Inverse Problems have always sought efficient and globally convergent numerical methods. The meaning of 'globally' is twofold. First, the numerical solution converges to a good approximation of the exact solution and is independent of the initial guess so long as this starting point is in an appropriate bounded set, which corresponds to the concept of compact set of the Tikhonov principle [40]. Second, a rigorous convergence analysis can be established for the numerical method that does not depend on small initial error. Minimization of a least-squares residual functional is commonly used for a Coefficient Inverse Problem. However, due to ill-posedness and high-nonlinearity, conventional residual least-squares functionals for such problems have multiple local minima and ravines [27]. Newton [14, 23, 32] and quasi-Newton methods [15, 34, 17] cannot guarantee convergence to the global minimum. Moreover, due to ill-posedness, there is no guarantee that the global minimum of such a functional is close to the true solution of the problem under consideration. This motivates the development of efficient numerical methods that converge globally and give fairly good approximate solutions for a broad class of Coefficient

Inverse Problems.

4 Convexification: The First Generation of Globally Convergent Numerical Methods

4.1 Earlier Work

The development of globally convergent methods for Coefficient Inverse Problems has root in the so-called convexification methods [26, 27, 28]. Such methods may be regarded as alternatives to the methods of global optimization, for instance, simulated annealing or genetic algorithms. Key ideas of the method were developed first in [26] for the one-dimensional coefficient inverse problem of electromagnetic frequency sounding of layered marine shallow water configurations. The method was extended to the multidimensional case in [28] with application to diffuse optical mammography. The monograph [27] records more details of the convexification method up to this stage. Global convergence theorems were rigorously proved in these publications. One version of the convexification algorithm was implemented for the two-dimensional problem of optical medical imaging where the light propagation process is governed by the elliptic equation $-\Delta u + a(\mathbf{x})u = \delta(\mathbf{x} - \mathbf{x}_0)$ with the unknown coefficient $a(\mathbf{x})$, $\mathbf{x} \in \mathbb{R}^3$ and where the source runs along a straight line [35].

The above mentioned convexification algorithms originate with the method of Carleman estimates for Coefficient Inverse Problems [9, 24, 27]. Prior to the convexification methods, Carleman estimates were not used for numerics but only for proofs of uniqueness and stability results. The main idea of the convexification is this. On a generic layer $\#j$, the Carleman weight function $\Psi_\lambda^j(z) := \exp[-\lambda(z - z_{j-1})]$ for the differential operator d^2/dz^2 is involved in the convexification procedure [43]. This sequence of weights has two functionalities: (1) ensuring the strict convexity of a j-dependent sequence of residual least-squares functionals, and (2) stabilizing the resulting layer stripping procedure. The strict convexity of these functionals is very important, since it ensures uniqueness of the global minimizer and absence of local minima. It is also well known that any gradient-like minimization method converges to this global minimum regardless of the starting point. In other words, the global convergence is guaranteed. Furthermore, the global convergence theorem guarantees that given the sequence of those minimizers, one can construct such an approximation to the unknown coefficient, which is close to the correct coefficient.

4.2 Further Development

Since the convexification algorithm involves quite a few parameters, it is imperative to conduct a systematic and comparative analysis on the effect of various parameters. Such study is valuable for the further development of the globally convergent algorithms and it was done in [43] with application to imaging of antipersonnel land mines and with four new ingredients to the algorithm itself. Compared with previous implementations of the convexification

algorithms, the four novel aspects are: (1) we minimize strictly convex functionals directly for each generic layer in the coordinate z direction instead of through the solution of an equivalent equation which is based on the contraction mapping operator, (2) based upon the preliminary study [41], a local basis which consists of cubic B-splines is applied in the spatial approximation, thus enabling sharper resolution of the reconstructed material property at the interface of inhomogeneities, (3) the so-called 'tails' in truncated integrals are fitted in to compensate the missing information, and (4) we approximate the functions that depend on the pseudo-frequency by Legendre polynomials, thus calculating the integrals involving pseudo-frequency explicitly rather than numerically.

One major advantage of the direct minimization of the convex functionals over solving an operator equation is that the time-consuming pre-programming and pre-computational effort to derive the operator equation is avoided. The numerical results in [43] show that the incorporation of tails in the convexification procedure substantially decreases the size of the interval for pseudo-frequency, in contrast to the previous 'tail-free' case [28], which requires a large interval in order to get acceptable accuracy for the recovered unknown coefficient. Thus, introduction of the tails has *dramatically* decreased the computational time. Further and more importantly, we have found that the tails are central and indispensable to the good accuracy of the convexification algorithm: in absence of the information from the tails, the quality of the reconstructed material property is rather poor though the location of the interface of the inhomogeneities has been identified rather well [43]. Thus, we believe that the incorporation of the tails in [43] is a *major* advancement to the convexification methods and further to the globally convergent methods. We mention that the first procedure of working with tails was proposed in subsection 5.4 of [18]. However, that was done for a different locally convergent algorithm.

Based on the valuable experience [43], the convexification algorithm has been further developed in [44], where the spatial x-approximation with cubic B-splines and the pseudo-frequency approximation with Legendre polynomials have been studied in greater details. Numerical results [44] have demonstrated that the new improvements in the convexification algorithm can improve identification of material properties and locations of the mines.

A smoothing technique [45] has been formally introduced to improve the quality of the reconstructed images based on the solution of the governing equations via the convexification algorithm. The idea is simple yet powerful and may be used in the broader area of image restoration and reconstruction. Since the recovered coefficient does not have enough smoothness, it is natural to seek a weak solution of the unknown coefficient rather than the strong one. The Galerkin method has been applied to obtain the weak solution of the recovered material property [45]. Reconstructed images of good quality have been shown for several different practical setups of land mines. The convexification algorithm is capable of imaging the spatially distributed dielectric permittivity function in: (1) the homogeneous background in absence of any inclusion, (2) homogeneous background with one single mine embedded, (3) homogeneous background with one mine and one stone embedded, (4) homogeneous background with two mines at two set of different locations and with two set of different sizes [45]. In all cases the value of the dielectric permittivity function in the

background and in inclusions was assumed to be unknown. An explanation for the artifacts in the reconstructed images has also been proposed based on numerical evidence [45].

To detect and image antipersonnel land mines in the battlefield in *real-time*, the numerical algorithm has to run fast, and this has been achieved in [46]. By properly choosing the upper limit for pseudo-frequency and with quadratic polynomial approximations of the quantities which depend on the pseudo-frequency, the convexification algorithm is highly efficient. On a standard workstation with a Linux operating system, the computational time for all realistic configurations of land mines is less than 10 seconds [46]. Such newly achieved efficiency allow the algorithm to be applied in *real-time* to detect and image mine-like targets in the field.

5 Frequency Convexification: The Second Generation of Globally Convergent Numerical Methods

The second generation of globally convergent numerical methods for Coefficient Inverse Problems has started recently from works [6, 4, 5]. Instead of using both Dirichlet and Neumann boundary conditions at a part of the boundary, this new method uses the Dirichlet boundary data at the entire boundary of a finite domain where the target coefficient is unknown [6]. Another feature with the new development is that the layer-stripping procedure is now with respect to the pseudo-frequency rather than with respect to the spatial variable of the convexification. Here the pseudo-frequency κ is a parameter proportional to the parameters of the Laplace transform of the original time dependent PDE. The layer stripping with respect to the pseudo frequency provides a better stability for the problem, thus enabling one to stably image larger domains of interest. On each thin κ-layer of the pseudo-frequency, the boundary value problem with the Dirichlet data for a nonlinear elliptic PDE of the second order is solved using the finite element method [6]. The Carleman weight function now depends on the pseudo-frequency rather than on the spatial variable. By properly choosing the parameter in the Carleman weight function, one can reduce the effect of the nonlinear term in each of these elliptic equations, thus, ending up with solving a linear problem for each iteration. Tails are also taken into account and are approximated via outer iterations. The algorithm with the new development [6] resembles the Landweber iteration [29]: on each step of the iteration, both the direct problem and the inverse problem are solved.

The most recent development in this direction is a synthesis of the globally convergent numerical method of [6] with the locally convergent so-called Finite Element Adaptive technique (adaptivity) [4, 5], see e.g., the references [1, 2, 3] for the adaptivity for inverse problems. This synthesis represents a two stage globally convergent numerical procedure. On the first stage a good first approximation for the unknown coefficient is found by the globally convergent numerical method of [6]. On the second stage this approximation is taken as a starting point for further refinement by the adaptivity technique. The adaptivity consists in applications of the quasi-Newton method on different meshes. First, this method is applied on the same mesh, on which the globally convergent parts has operated. It was shown numerically in [4, 5] that this application does not lead to a refinement of the image.

Next, the true substance of the adaptivity comes in. Namely, *a posteriori* error analysis of the computed image shows sub-domains of the original domain where the maximal error of the solution is. It is important that one does not need to know the solution in advance to do this error analysis. Instead one needs to know only an upper estimate for the solution. So, the mesh is refined in those sub-domains and the quasi-Newton method is applied again. Usually the process stops after 3-4 mesh refinements when the image is stabilized. It was shown numerically in [4, 5] that reconstructions are improved in this way. An alternative to local mesh refinement would be to use a very fine finite element mesh in the entire domain of interest. However, this would impose excessive requirements on capabilities of computers.

6 Computational Results

In this section we briefly sample our results both with the convexification algorithms [43, 44, 45, 46] and with the new development [6, 4, 5]. For all the technical details of the methods, we refer the reader to the original references.

6.1 Results from the Convexification Algorithms

First we describe a mathematical model for the Coefficient Inverse Problem of detection and imaging of antipersonnel land mines that are buried under the ground. Some assumptions and simplifications have been made with our model. At the same time we use realistic ranges of parameters. First, we work with a two-dimensional model. The irregularity of the ground surface has been neglected to avoid the complication of gathering the data for the direct problem. Also, we assume that the dielectric permittivity ε of the medium does not have a discontinuity at the ground surface where measurements of the back reflected electric signal are performed. Further, we neglect the electric conductivity of the medium, which can be justified in the case when the background is a dry soil [18].

Now, suppose a polarized electric field is generated by an above-ground pulse at the point $\mathbf{x}_0 = (0, -|\xi|)$ at the initial time $t = 0$, where $\xi \neq 0$. The following hyperbolic equation can be derived from the Maxwell equations [11]

$$-\mu\varepsilon(\mathbf{x})u_{tt} + \Delta u = 0,\ (\mathbf{x}, t) \in \mathbb{R}^2 \times \mathbb{R}^+, \tag{1}$$

$$u(\mathbf{x}, 0) = 0,\ u_t(\mathbf{x}, 0) = \delta(\mathbf{x} - \mathbf{x}_0), \tag{2}$$

where $\mathbf{x} = (x, z)$, the function $u(\mathbf{x}, t)$ is one component of the electric field, the parameter $\mu = 4\pi \times 10^{-7}\,(Henry/m)$ is the magnetic permeability in free space, $\varepsilon = \varepsilon_0\varepsilon_r(\mathbf{x})$ is the dielectric permittivity, $\varepsilon_0 \approx 8.854 \times 10^{-12}\,(Farad/m)$ is the dielectric permittivity of free space and $\varepsilon_r(\mathbf{x})$ is the dimensionless relative dielectric permittivity of the medium.

In both dry soil and trinitrotoluene (TNT) we have $\varepsilon_r \approx 2.9$ [18]. We are interested in the identification of antipersonnel plastic mines, which is difficult in a practical scenario since the metal component in them is not large. Hence, we need one parameter inside the mine which can give us sufficient contrast against the surrounding dry soil. It is well-known

that a large portion of the volume of any mine is filled with air and $\varepsilon_r = 1$ for the air. As the mine does not wholly consist of air, it is reasonable to assume that $\varepsilon_r = 1.5$ inside the mine, which is about the average value of the coefficient ε_r within the mine. Thus, for our simulation we assume

$$\varepsilon_r(\mathbf{x}) = \begin{cases} 2.9 \text{ outside mines} \\ 1.5 \text{ inside mines} \end{cases} \tag{3}$$

The sizes of antipersonnel mines usually vary between 5 cm and 10 cm, and they lay at a small depth underneath the ground, not exceeding 10 cm. So we model mines as disks of radius 5 cm which are located in the range $z \in [0, 9]$ cm.

If one can quantify the coefficient $\varepsilon_r(\mathbf{x})$, then points whose values are close to 1.5 will be those inside or close to the mine. Thus, finding an approximation for this coefficient by solution of the Coefficient Inverse Problem (below) would provide us useful information about a target which we would 'suspect' is a land mine.

To solve the problem in the framework of the convexification method, we consider the Laplace transform of the function $u(\mathbf{x}, t)$

$$w(\mathbf{x}, s) = \mathcal{L}\left[u(\mathbf{x}, t)\right] := \int_0^\infty u(\mathbf{x}, t) e^{-st} dt.$$

Because the physical parameters μ and ε_0 are very small, by combining them with the parameter s we rescale these two parameters and introduce a new variable $\kappa := s\sqrt{\mu\varepsilon_0}$, which is termed 'pseudo-frequency'. Equations (1) and (2) transform into

$$-\Delta w + \kappa^2 \varepsilon_r(\mathbf{x}) w = \delta\left(\mathbf{x} - \mathbf{x}_0\right), \ \mathbf{x} \in \mathbb{R}^2, \tag{4}$$

$$\lim_{|\mathbf{x}| \to \infty} w(\mathbf{x}, \kappa) = 0. \tag{5}$$

Coefficient Inverse Problem (CIP). Consider a rectangle $\Omega \subset \mathbb{R}^2$

$$\Omega := \left\{-A < x < A, \ z \in (0, L)\right\}, \ A, L > 0.$$

Suppose the coefficient $\varepsilon_r(\mathbf{x})$ of the equation (4) is unknown in Ω and known in $\mathbb{R}^2 \diagdown \Omega$. Determine the relative dielectric permittivity $\varepsilon_r(\mathbf{x})$ for $\mathbf{x} \in \Omega$, assuming the following two functions $\varphi(x, \kappa)$ and $\psi(x, \kappa)$ are known for a single source position $\mathbf{x}_0$

$$w(x, 0, \kappa) = \varphi(x, \kappa), \ w_z(x, 0, \kappa) = \psi(x, \kappa), \ \forall (x, \kappa) \in (-A, A) \times [\kappa_0, \bar{\kappa}]. \tag{6}$$

We now need to decide the lower limit κ_0 and upper limit $\bar{\kappa}$ of pseudo-frequency κ for our inverse problem. To find an appropriate constant $\bar{\kappa}$, we compute solutions of the forward problem (4), (5) for different values of the parameter $\kappa > 0$ and determine such a value $\kappa := \bar{\kappa}$, beyond which the asymptotic behavior, i.e., exponential decay, of the function $w(\mathbf{x}, \kappa)$ holds. In this case the function $\ln\left[w(\mathbf{x}, \kappa)\right]$ should be close to a linear function with respect to κ. Thus, we identify such values of κ for which

$$\ln\left[w(\mathbf{x}, \kappa)\right] = v(\mathbf{x}, \kappa) \approx c_1(\mathbf{x})\kappa + c_0(\mathbf{x}) \tag{7}$$

for many points $\mathbf{x} \in \overline{\Omega}$. The function $v(\mathbf{x}, \kappa)$ looks like a straight line with respect to κ for $\kappa > \bar{\kappa}$. We solve the forward problem on a large domain $\Xi := \{-6 \leq x, z \leq 6\}$ using the finite element package - COMSOL $Multiphysics^{TM}$ version 3.2. A zero Dirichlet boundary condition is imposed on the boundary $\partial\Xi$. We use triangular elements with Lagrange cubic basis. The mesh is quasi-uniform and locally refined near the source location $\mathbf{x}_0 = (0, -0.1)$ with 38,944 elements, see Figure 1. The total degrees of freedom are 351,218. We obtain $\bar{\kappa} = 10$ after rounding to integers. One is free to choose the lower bound κ_0. We may take a smaller value that is close to $\bar{\kappa}$, e.g., $\kappa_0 = \{8, 9\}$. The influence of the lower limit κ_0 on the resolution of the recovered unknown coefficient ε_r can be seen below.

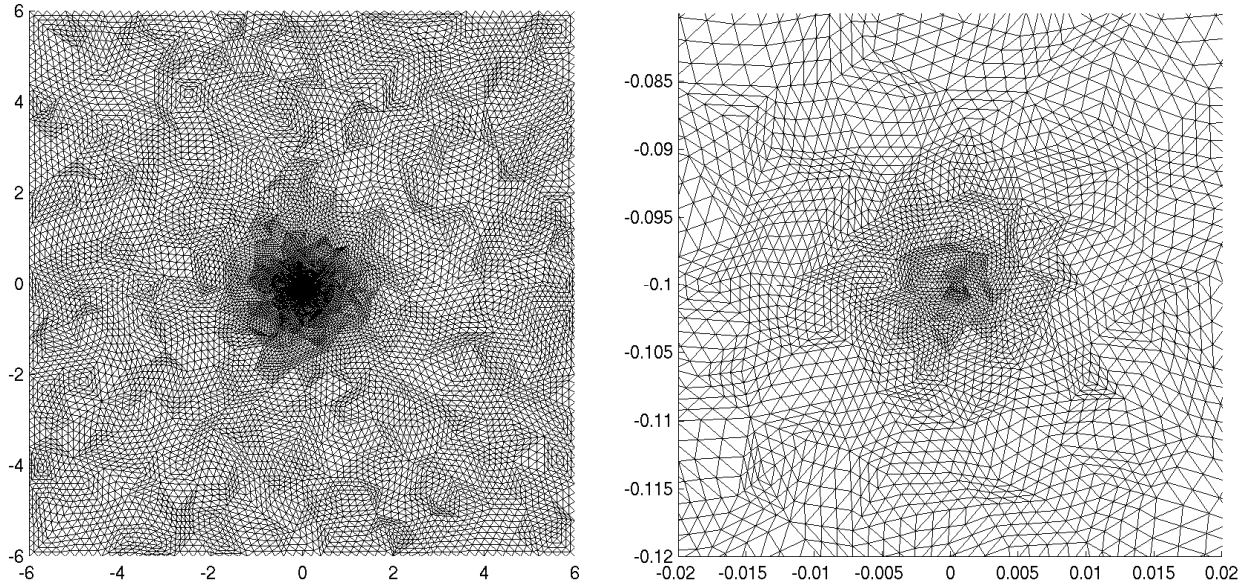

Figure 1: Quasi-uniform (left) and locally refined (right) mesh for the forward problem.

To make the problem even harder, we have added in another inclusion, a small stone. To differentiate between the stone and the dry soil, we accept a notion that the stone is slightly wet, which might be a result of a past rain. Thus, we take $\varepsilon_r \approx 4$ in the stone [18]. We model the stone as a disk with radius of 5 cm and $\varepsilon_r = 4.0$ in it. The center of the stone is located at the point $P_s = (-0.4, 0.075)$, i.e., the same depth 7.5 cm underneath the ground as the mine, whose center is at the point $P_m = (0.4, 0.075)$. The x-interval for the inverse problem is $\Omega_x := [-A, A] = [-0.7, 0.7]$. The computation is performed with 51 splines with uniform layer size $\delta z = 5$ mm. Functions which depend on the pseudo-frequency are approximated with Legendre polynomials of degree 5. The parameter λ which is associated with the Carleman weight function is set to 200. The threshold δ to terminate the steepest descent method takes the value of 0.01. For the effects of various parameters on the reconstructed material property, we refer the reader to the systematic study [43]. The main procedure in the convexification algorithm is described as follows.

Convexification Algorithm

1. Solve the forward problem (4) to obtain initial data $\vec{a}_1^{(0)}$, $\vec{b}_1$, $\vec{c}_1$ and tails $\vec{\chi}_1$, $\vec{\chi}_1'$; $j = 1$
2. Minimize the objective function F_λ^j for the unknown $\vec{a}_j$ in layer # j
3. Update the initial data $\vec{a}_{j+1}^{(0)}$, $\vec{b}_{j+1}$, $\vec{c}_{j+1}$ and tails $\vec{\chi}_{j+1}$, $\vec{\chi}_{j+1}'$ for next layer # $j+1$; $j+1 \to j$
4. Repeat 2., 3., until $j = N$, the number of total layers
5. Reconstruct the unknown coefficient $\varepsilon_r(\mathbf{x})$ for all layers

At each generic layer $z \in (z_{j-1}, z_j]$, the objective function to be minimized has the form

$$F_\lambda^j\left(\vec{a}_j(\kappa)\right) = \int\limits_{\kappa_0}^{\bar{\kappa}} d\kappa \int\limits_{z_{j-1}}^{z_j} \Phi^2\left[\widetilde{p}_j\left(\vec{a}_j(\kappa), z, \kappa\right), \kappa\right] \Psi_\lambda^j(z)\, dz, \tag{8}$$

where $\vec{a}_j$ is the unknown vector to be found, Φ is the system of nonlinear ordinary integral-differential equations which result from spatial- and pseudo-frequency approximations, and $\widetilde{p}_j$ is the function from the layer-stripping procedure and depends on the unknown vector $\vec{a}_j$. We refer the reader to the publications [43, 44, 45, 46] for more details.

Figure 2 shows the results for our computation. A very good solution accuracy is evident. There is neither overshoot near the stone nor undershoot near the mine. The stone, the background medium and the mine have been correctly and sharply identified in terms of their locations and material property. The difference shows up on both blow-up views. The performance of the reconstructed ε_r is a little better with $\kappa_0 = 8$. This is due to the extra information with κ integration for $\kappa \in [8, 9]$, which is present when $\kappa_0 = 8$ and which is lost in the case $\kappa_0 = 9$.

6.2 A synthesis of globally convergent numerical method with adaptivity technique

In this section we describe some results of the globally convergent numerical method in combination with the adaptivity technique presented in [6, 4, 5].

6.2.1 Computations of the Forward Problem and statement of Inverse Problem

We work with the computationally simulated data which are generated by computing the forward problem (10) with the given function $c(x)$. To solve the forward problem, we use the hybrid FEM/FDM method described in [7]. The computational domain in all our two-dimensional tests is $G = G_{FEM} \cup G_{FDM}$ and is set as $G = [-4.0, 4.0] \times [-5.0, 5.0]$. This domain is split into a finite element domain $G_{FEM} := \Omega = [-3.0, 3.0] \times [-3.0, 3.0]$ and

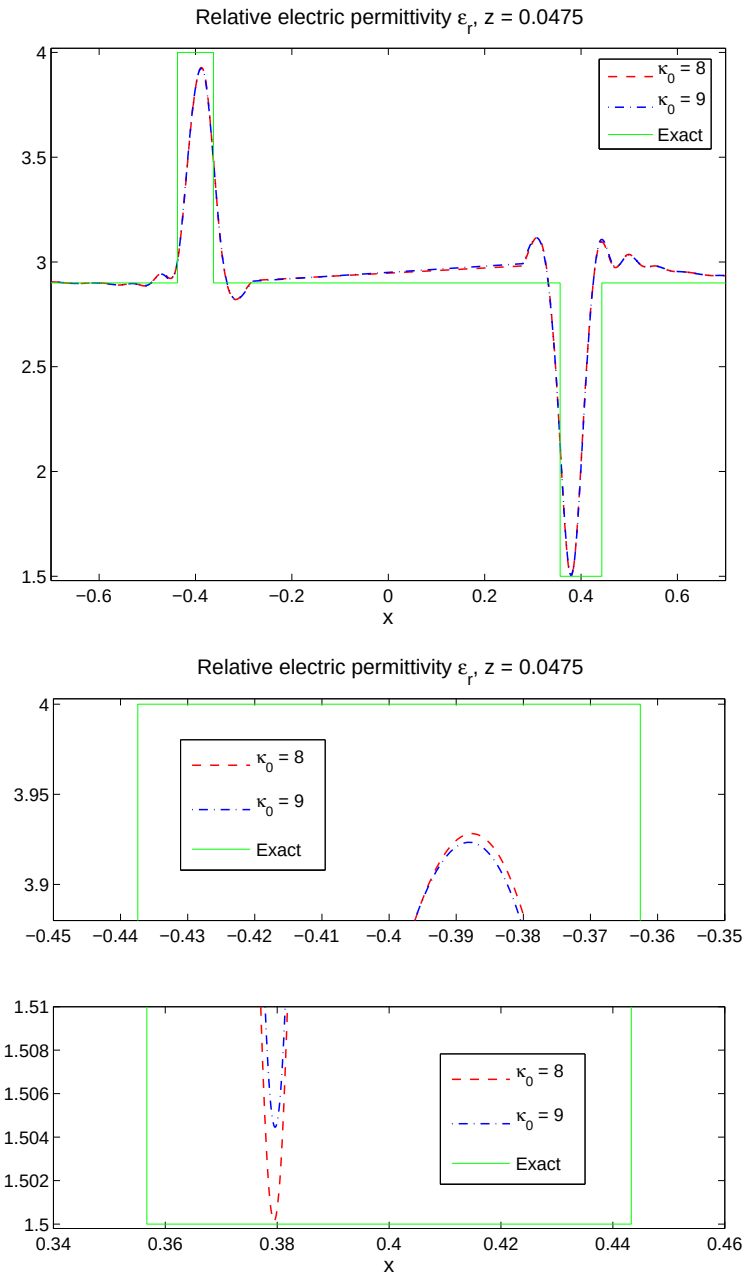

Figure 2: Cross-sectional views of relative electric permittivity ε_r for the case of stone $\oplus$ mine against background. Two different values of κ_0 are considered. The depth underneath the ground is $z = 4.75$ cm. Top: normal-scale view. Middle: blow-up view near the stone. Bottom: blow-up view near the mine.

a surrounding domain G_{FDM} with a structured mesh, see Figure 3. The computational domain in all our three-dimensional tests is $G = G_{FEM} \cup G_{FDM}$ and is set as $G = [-4.0, 4.0] \times$

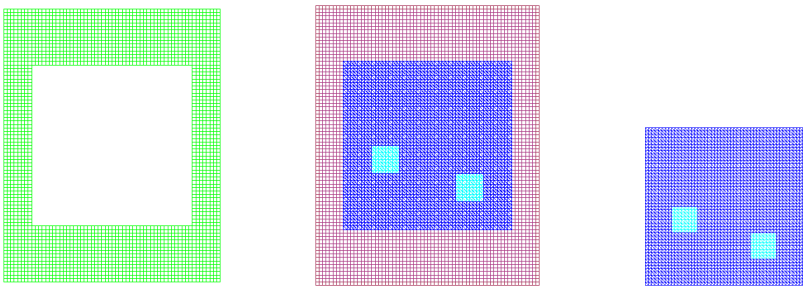

(a) G_{FDM} (b) $G = G_{FEM} \cup G_{FDM}$ (c) $G_{FEM} = \Omega$

Figure 3: The hybrid mesh (b) is a combinations of a structured mesh (a), where FDM is applied, and a mesh (c), where we use FEM, with a thin overlapping of structured elements. The solution of the inverse problem is computed in the square Ω and $c(x) = 1$ for $x \in G \diagdown \Omega$.

$[-5.0, 5.0] \times [-2.5, 2.0]$. This domain is split into a finite element domain $G_{FEM} := \Omega = [-3.0, 3.0] \times [-3.0, 3.0] \times [-2.0, 1.5]$ and a surrounding domain G_{FDM} with a structured mesh. The forward problem in two and three dimensional examples is computed in the domain $G \subset \mathbb{R}^n, n = 2, 3$. The coefficient $c(x)$ is unknown only in domain $\Omega \subset G$ and

$$c(x) = 1 \text{ in } G \diagdown \Omega. \tag{9}$$

The trace of the solution of the forward problem is recorded at the boundary ∂G. Next, the coefficient $c(x)$ is "forgotten", and our goal is to reconstruct this coefficient for $x \in \Omega$ from the data $\varphi(x, s)$. The boundary of the domain G is $\partial G = \partial G_1 \cup \partial G_2 \cup \partial G_3$. Here, ∂G_1 and ∂G_2 are respectively top and bottom sides of the largest domain of Figure 3 and ∂G_3 is the union of left and right sides of this domain. In our test the forward problem is

$$\begin{aligned} c(x)\frac{\partial^2 u}{\partial t^2} - \triangle u = 0, \quad & \text{in } G \times (0, T), \\ u(\cdot, 0) = 0, \ \frac{\partial u}{\partial t}(\cdot, 0) = 0, \ & \text{in } G, \\ \partial_n u\big|_{\partial G_1} = f(t), \ & \text{on } \partial G_1 \times (0, t_1], \\ \partial_n u\big|_{\partial G_1} = \partial_t u, \ & \text{on } \partial G_1 \times (t_1, T), \\ \partial_n u\big|_{\partial G_2} = \partial_t u, \ & \text{on } \partial G_2 \times (0, T), \\ \partial_n u\big|_{\partial G_3} = 0, \ & \text{on } \partial G_3 \times (0, T), \end{aligned} \tag{10}$$

where T is the final time and $f(t)$ is the plane wave defined as

$$f(t) = \frac{(\sin(\overline{s}t - \pi/2) + 1)}{10}, \ 0 \le t \le t_1 := \frac{2\pi}{\overline{s}}, T = 17.8 t_1.$$

6.2.2 Description of the globally convergent numerical method of [6]

Let us consider the Cauchy problem for a hyperbolic PDE

$$c(x)\,u_{tt} = \Delta u \text{ in } \mathbb{R}^3 \times (0,\infty), \tag{11}$$
$$u(x,0) = 0, u_t(x,0) = \delta(x - x_0). \tag{12}$$

Let d_1 and d_2 be two positive constants and $\Omega \subset \mathbb{R}^3$ be a convex bounded domain with the boundary $\partial\Omega \in C^3$. We assume that the coefficient $c(x)$ of equation (11) is such that

$$c(x) \in [d_1, 2d_2], d_1 < d_2, c(x) = 2d_1 \text{ for } x \in \mathbb{R}^3 \setminus \Omega, \tag{13}$$
$$c(x) \in C^2\left(\mathbb{R}^3\right). \tag{14}$$

We consider the following

Inverse Problem. Suppose that the coefficient $c(x)$ satisfies (13) and (14), where the positive numbers d_1 and d_2 are given. Assume that the function $c(x)$ is unknown in the domain Ω. Determine the function $c(x)$ for $x \in \Omega$, assuming that the following function $g(x,t)$ is known for a single source position $x_0 \notin \overline{\Omega}$

$$u(x,t) = g(x,t), \forall (x,t) \in \partial\Omega \times (0,\infty). \tag{15}$$

Consider the Laplace transform of the functions u,

$$w(x,s) = \int_0^\infty u(x,t)e^{-st}dt, \text{ for } s > \underline{s} = const. > 0, \tag{16}$$

where $\underline{s}$ is a certain number. It is sufficient to choose $\underline{s}$ such that the integral (16) would converge together with corresponding (x,t)-derivatives. We call the parameter s *pseudo frequency*. Note that we do not use the inverse Laplace transform in our method, since approximations for the unknown coefficient are obtained in the pseudo frequency domain. Since by the maximum principle $w(x,s) > 0$, then we can consider the function $q(x,s) = \partial_s(s^{-2}lnw(x,s))$. This function satisfies a certain nonlinear integral differential equation with Volterra integrals with respect to s, where integration is carried out from s to $\bar{s}$, where $\bar{s}$ is the value of the pseudo frequency at which these integrals are truncated. In that equation the so- called tail function is also involved. This function complements that truncation, it is unknown and it is small because of a certain asymptotic behaviour at $\bar{s} \to \infty$. Therefore that equation contains two unknown functions q and the tail. The reason why we can approximate both of them is that we treat them differently: while the function q is approximated via inner iterations, the tail function is approximated via outer iterations. Consider a partition of the interval into small subintervals with the length of h. Approximate the function q as a piecewise constant function q_n with respect to s on each of these small intervals $(s_n, s_{n-1}]$. Next, the equation for q_n is multiplied by the Carleman Weight Function $CWF = e^{\mu(s-s_{n-1})}$, where μ is a large parameter. Then the resulting equation is integrated

with respect to $s \in (s_n, s_{n-1}]$. As a result, a finite sequence of Dirichlet boundary value problems for nonlinear elliptic PDEs for functions q_n is obtained, where Dirichlet boundary conditions are known. This system is solved sequentially. As soon as the function q_n is approximated, an approximation c_n for the unknown coefficient c is found and the next update for the tail function is also found. The first approximation for the tail is either zero or the one which corresponds to the solution of the above Cauchy problem for $c = 2d_1$. Let σ be a small parameter characterizing the level of the error in the data, and ϵ be a certain small regularization parameter which is introduced to improve the stability property of solving the above Dirichlet boundary value problems. Let $\xi > 0$ be a small number such that certain norm of the tail is less than ξ. Denote $\eta = 2(h + \sigma + \epsilon + \xi)$. Then η is small. The global convergence theorem of [6] claims that $|c_n - c^*|_\alpha \leq C\eta$, where $|\cdot|_\alpha$ is a Hölder norm, c^* is the exact solution of our CIP satisfying (11), (12) and $C > 0$ is a constant. Thus, the globally convergent part provides a good approximation for the exact solution.

6.2.3 The Adaptivity Technique

To use the adaptivity technique, we formulate the inverse problem for the boundary value problem (10) as an optimization problem, where we seek the unknown coefficient $c(x)$, which gives the solution of the boundary value problem (10) for the function $u(x,t)$ with the best least squares fit to the time domain observations $g(x,t)$, see (15). Denote $Q_T = \Omega \times (0,T), S_T = \partial\Omega \times (0,T)$. Our goal now is to find the function $c(x)$ which minimizes the Tikhonov functional

$$E(u,c) = \frac{1}{2}\int\limits_{S_T} (u\mid_{S_T} - g(x,t))^2 d\sigma dt + \frac{1}{2}\gamma \int\limits_{\Omega} (c - c_0)^2 \ dx, \tag{17}$$

where γ is the regularization parameter and c_0 is an initial guess for the unknown coefficient c which was obtained on the globally convergent stage.

Denote

$$\begin{aligned}
H_u^2(Q_T) &= \{f \in H^2(Q_T) : f(x,0) = f_t(x,0) = 0\},\\
H_u^1(Q_T) &= \{f \in H^1(Q_T) : f(x,0) = 0\},\\
H_\varphi^2(Q_T) &= \{f \in H^2(Q_T) : f(x,T) = f_t(x,T) = 0\},\\
H_\varphi^1(Q_T) &= \{f \in H^1(Q_T) : f(x,T) = 0\},\\
U &= H_u^2(Q_T) \times H_\varphi^2(Q_T) \times C^2(\overline{\Omega}),\\
\bar{U} &= H_u^1(Q_T) \times H_\varphi^1(Q_T) \times L_2(\Omega),\\
\bar{U}^1 &= L_2(Q_T) \times L_2(Q_T) \times L_2(\Omega),
\end{aligned} \tag{18}$$

where all functions are real valued. Hence, $U \subset \bar{U} \subset \bar{U}^1$ as sets, U is dense in $\bar{U}$ and $\bar{U}$ is dense in $\bar{U}^1$. Also denote $((\cdot,\cdot))$ the inner product in $\bar{U}^1$ and $[\cdot]$ the norm generated by this product.

To solve the problem of the minimization of the functional (17), we introduce the Lagrangian

$$L(v) = E(u,c) + \int\limits_{Q_T} \varphi \cdot (cu_{tt} - \Delta u)\, dxdt, \forall \varphi \in H^2_\varphi(Q_T), \tag{19}$$

where $\varphi \in H^2_\varphi(Q_T)$ is the Lagrange multiplier and $v = (u, \varphi, c) \in U$. Since the function u solves equation (10) then $L(v) = E(u,c)$. Integration by parts and (19) leads to

$$L(v) = E(u,c) - \int\limits_{Q_T} c(x) u_t \varphi_t dxdt + \int\limits_{Q_T} \nabla u \nabla \varphi dxdt - \int\limits_{S_T} p\varphi d\sigma dt. \tag{20}$$

We search for a stationary point of the functional $L(v), v \in U$ satisfying

$$L'(v)(\overline{v}) = 0, \quad \forall \bar{v} = (\bar{u}, \bar{\varphi}, \bar{c}) \in \bar{U} \tag{21}$$

where $L'(v)(\cdot)$ is the Frechet derivative of L at the point v. We obtain from (20) and (21)

$$L'(v)(\overline{v}) = \int\limits_\Omega \bar{c} \left[\gamma (c - c_0) - \int\limits_0^T u_t \varphi_t dt \right] dx - \int\limits_{Q_T} c(x) \left(\varphi_t \overline{u}_t + u_t \overline{\varphi}_t \right) dxdt \tag{22}$$

$$+ \int\limits_{Q_T} (\nabla u \nabla \overline{\varphi} + \nabla \overline{u} \nabla \varphi) - \int\limits_{S_T} p \overline{\varphi} d\sigma dt - \int\limits_{S_T} (g - u|_{S_T}) \overline{u} d\sigma dt = 0, \forall \bar{v} = (\overline{u}, \overline{\varphi}, \overline{c}) \in \bar{U}.$$

Integrating by parts in (22) we obtain that if $(u, \varphi, c) = v \in U$ is a minimizer of the Lagrangian $L(v)$ in (20), then

$$cu_{tt} - \triangle u = 0, (x,t) \in Q_T, \tag{23}$$

$$u(x,0) = u_t(x,0) = 0, \tag{24}$$

$$\partial_n u \mid_{S_T} = p(x,t); \tag{25}$$

$$c\varphi_{tt} - \triangle \varphi = 0, (x,t) \in Q_T, \tag{26}$$

$$\varphi(x,T) = \varphi_t(x,T) = 0, \tag{27}$$

$$\frac{\partial \varphi}{\partial n} \mid_{S_T} = (g - u)(x,t), (x,t) \in S_T; \tag{28}$$

$$\gamma(c - c_0) - \int_0^T u_t \varphi_t \, dt = 0, x \in \Omega. \tag{29}$$

The boundary value problem (26)-(28) should be solved backwards in time.

6.2.4 The adaptive algorithm

In this section we present our adaptive algorithm based on computations of the residuals for the computed coefficient c. More details about a posteriori error estimate for the unknown coefficient can be found in [3, 4, 5].

Adaptive algorithm

0. Choose an initial mesh K_h and an initial time partition J_0 of the time interval $(0, T]$. Start with an initial guess $c_0 = c_{glob}$, which was computed in the above globally convergent algorithm, and compute the sequence of c^m in the following steps:

1. Compute the solution u^m of the forward problem (23)-(25) on K_h and J_k, with $c(x) = c^m$.

2. Compute the solution φ^m of the adjoint problem (26)-(28) backwards in time on K_h and J_k.

3. Update the coefficient $c := c_h$ on K_h and J_k using the quasi-Newton method

$$c^{m+1} = c^m - \alpha H^m g^m.$$

4. Stop computing c if either the norm of the gradient g^m of the Lagrangian with respect to the coefficient in (29) is $||g^m||_{L_2(\Omega)} < \theta$ or norms $||g^n||_{L_2(\Omega)}$ are stabilized. Otherwise set $m = m + 1$ and go to step 1. Here, θ is the tolerance in quasi-Newton updates. In our computations we took $\theta = 10^{-5}$.

5. Compute the residuals, R_{c_1}, R_{c_2}, where $R_{c_1}(x,t) = \left|\frac{\partial \varphi_h}{\partial t}\right| \cdot \left|\frac{\partial u_h}{\partial t}\right|$, $R_{c_2} = \gamma|(c_h - c_0)|$, and refine the mesh at all points where

$$\int_0^T \left(\max_{\overline{\Omega}} R_{c_1}(x,t) + \max_{\overline{\Omega}} R_{c_2}(x,t) \right) dt > tol. \tag{30}$$

   Here *tol* is a tolerance chosen by the user.

6. Construct a new mesh K_h and a new time partition J_k. On J_k the new time step τ should be chosen with respect to the CFL condition. Interpolate the reconstructed coefficient c_h from the previous mesh to the new mesh. Return to the step 1 and perform all the steps of the optimization algorithm on the new mesh.

6.2.5 Results of reconstruction in 2-d using the globally convergent algorithm

We have performed numerical experiments to reconstruct the medium, which is homogeneous with $c(x) = 1$ except of two small squares, where $c(x) = 4$, see Figure 3-c).

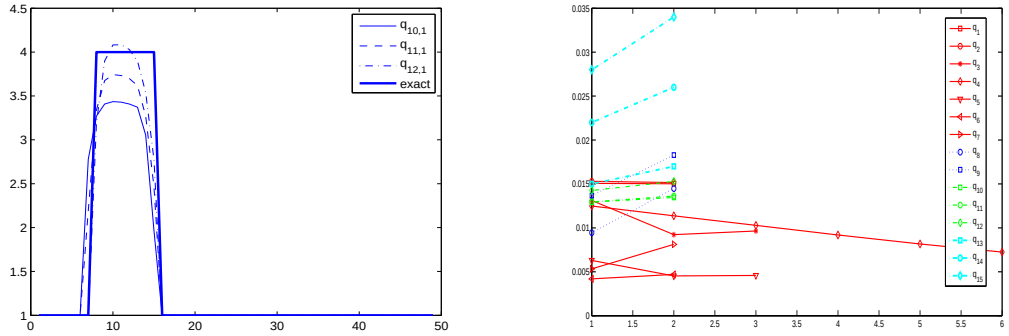

a) b)

Figure 4: Two-dimensional example of [4]. The one-dimensional cross-sections of the image of the function $c_{n,k}$. On a) along the vertical line passing through the middle of the right small square computed for corresponding functions $q_{n,1}$; and on b) computed L_2-norms of the $F_{n,i} = ||q_{n,i} \mid_{\partial\Omega} - q_{exact}||_{L_2(\partial\Omega)}$.

It was found in [6] that for domains G, Ω specified in section 7 the interval $[\underline{s}, \overline{s}] = [6.7, 7.45]$ is the optimal one, and so we have used it in our numerical studies. We have chosen the step size with respect to the pseudo frequency $h = 0.05$.

Once the function q_n is calculated, we update the function $c := c_n$, see subsection 7.3 of [6] for some numerical details. The resulting computed function is $c(x) := c_{\overline{N}}(x)$.

Figure 4-a) presents the one-dimensional cross-sections of computed functions $c_{n,k}$ superimposed with the correct one along the vertical line passing through the middle of the right small square. Comparison of images of functions $c_{n,k}$ for different values n and k shows that the inclusion/background contrasts grow with the grow of n and k.

One can see from Figure 5-b) that the $3.8 : 1$ contrast in the right square is imaged for $n := \overline{N} = 12$. However, location of the left square is shifted downwards, and both imaged squares are on about the same horizontal level. Values of the function $c(x) = 1$ outside of these squares are also imaged accurately.

6.2.6 The synthesis of the globally convergent algorithm with the adaptivity

The adaptive algorithm means, that we find the solution of our problem in an iterative process, where we start with a coarse mesh shown on Figure 5-a), find an approximate solution by the quasi-Newton method on this mesh. Next, we evaluate residuals regarding to the computed coefficient and refine the mesh locally at those regions where residuals have largest values, construct a new mesh and a new time partition, and repeat the computations again on this new mesh. We stop iterative process when L_2-norms of the computed gradient for the coefficient are stabilized or started to increase for all further refinements of the mesh, see [4, 5] for full details of our adaptive algorithm.

We test the synthesis of both globally convergent and adaptive methods with the starting

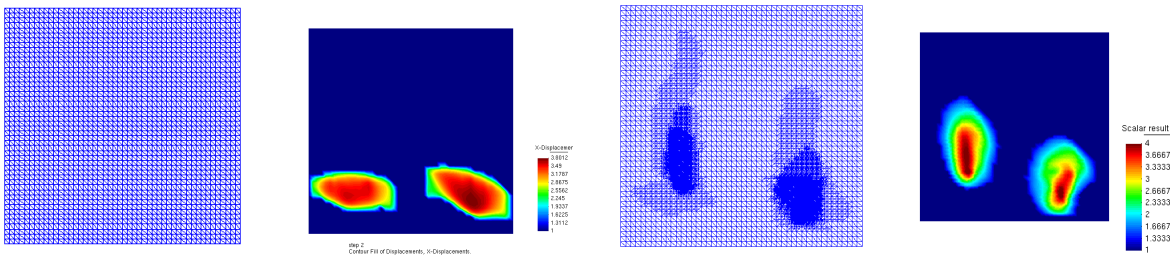

a) 4608 elements b) 4608 elements c) 23344 elements d) 23344 elements

Figure 5: Two-dimensional example of [4]. On a) we present coarse mesh and on b) spatial distributation of c_h obtained at the first stage of the above globally convergent procedure. On c) we show finaly adaptively refined computational mesh of the second stage, and on d) correspondingly distribution of the parameter c_h with noise level $\sigma = 0\%$ in data.

opt.it.	4608 elements	5340 elements	8230 elements	14604 elements	23344 elements
1	0.0193568	0.0167242	0.0146001	0.0131787	0.0224184
2	0.0193944	0.0157746	0.0139716	0.0133006	0.0208246
3		0.0133565			0.0208889
4		0.0125237			0.0204343

Table 1: Test 1.2: $||u\ |_{\Gamma_T} - g||_{L_2(\Gamma_T)}$ on adaptively refined meshes. The number of stored corrections in quasi-Newton method is $n = 15$. Computations was performed with the noise level $\sigma = 0\%$ and with the regularization parameter $\gamma = 0.01$.

point on the coarse mesh taken from the results of the first stage of our two-stage globally convergent procedure. More precisely, as the starting point for the coefficient $c(x)$ in the adaptive algorithm on the coarse mesh we take $c_{12,2}$, which corresponds to Figure 5-b). Testing was performed on 4 times adaptively refined meshes and with introducing $\sigma = 0\%$ and $\sigma = 5\%$ of the multiplicative random noise in the function $g(x,t)$ in an adaptive procedure, see [4]. In Table 1 we present computed L_2-norms of $||u\ |_{\Gamma_T} - g||_{L_2(\Gamma_T)}$ in the quasi-Newton method for adaptively refined meshes. We observe that these norms decrease as meshes are refined. Then they slightly increase and are finally stabilized for all refinements $n > 3$ of the initial mesh. Figures 5-c),d) show that the adaptivity technique enhances the quality of the reconstruction obtained on the first stage. We conclude that at the second stage of our two-stage procedure we are able to reconstruct well locations of both small squares.

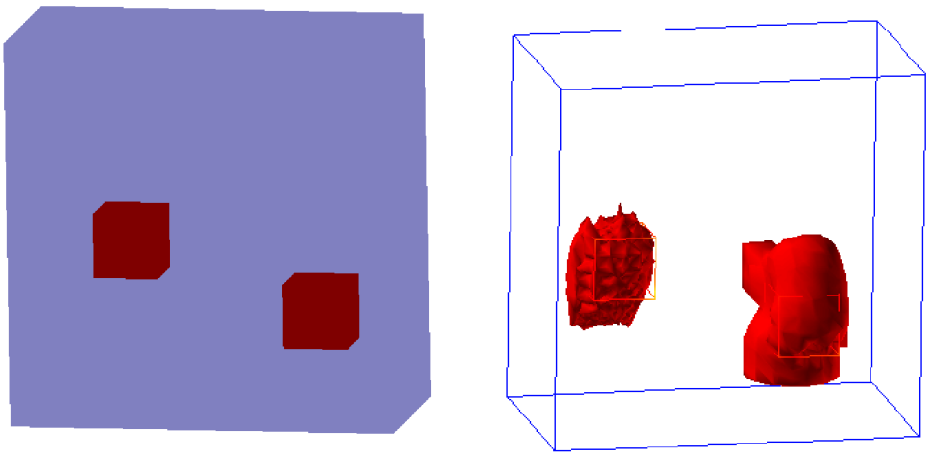

Figure 6: Three-dimensional example of [5]. Measurements of the outcome time dependent wave field are taken at the boundary of a prism. On a) we present the real image and on b) spatial distributation of c_h obtained by the two stage globally convergent numerical procedure. Both locations of inclusions and values of the unknown coefficient inside and outside of them are accurately imaged.

7 Concluding Remarks

The globally convergent methods are still being refined to make the algorithms more stable, robust and accurate. The methods can be applied to a broad class of Coefficient Inverse Problems. It is anticipated that more and more applications in science and engineering will be tackled by these techniques.

8 Acknowledgment

This research was supported by the U.S. Army Research Laboratory and U.S. Army Research Office under grants number W911NF-05-1-0378 and W911-08-1-0470.

References

[1] L. Beilina and C. Clason. An adaptive hybrid FEM/FDM method for an inverse scattering problem in scanning acoustic microscopy. *SIAM J. Sci. Comput.*, 28(1):382–402, 2006.

[2] L. Beilina and C. Johnson. Hybrid FEM/FDM method for inverse scattering problem. In *ENUMATH 2001*, Springer-Verlag, 2001.

[3] L. Beilina and C. Johnson. Hybrid FEM/FDM method for inverse scattering problem. *Mathematical Models and Methods in Applied Sciences*, 15(1):23–37, 2005.

[4] L. Beilina and M. V. Klibanov. A globally convergent numerical method and adaptivity for a hyperbolic coefficient inverse problem. submitted for publication in 2009, available on-line at http://www.ma.utexas.edu/mp_arc/.

[5] L. Beilina and M. V. Klibanov. Synthesis of global convergence and adaptivity for a hyperbolic coefficient inverse problem in 3D. submitted for publication in 2009, available on-line at http://www.ma.utexas.edu/mp_arc/.

[6] L. Beilina and M. V. Klibanov. A globally convergent numerical method for a coefficient inverse problem. *SIAM J. Sci. Comput.*, 31(1):478–509, 2008.

[7] L. Beilina, K. Samuelsson, and K. Åhlander. Efficiency of a hybrid method for the wave equation. In *FEM3D*, Gakuto International Series Mathematical Sciences and Applications. Gakkotosho CO., 2001.

[8] L. Bourgeois. Convergence rates for the quasi-reversibility method to solve the Cauchy problem for Laplace's equation. *Inverse Problems*, 22(2):413–430, 2006.

[9] A. L. Bukhgeim and M. V. Klibanov. Uniqueness in the large of a class of multidimensional inverse problems. *Soviet Math. Dokl.*, 17:244–247, 1981.

[10] H. Cao, M. V. Klibanov, and S. V. Pereverzev. A Carleman estimate and the balancing principle in the quasi-reversibility method for solving the Cauchy problem for the Laplace equation. *Inverse Problems*, 25(3):035005, 21 pp., 2009.

[11] M. Cheney and D. Isaacson. Inverse problems for a perturbed dissipative half-space. *Inverse Problems*, 11:865–888, 1995.

[12] M. Cheney, D. Isaacson, and J. C. Newell. Electrical impedance tomography. *SIAM Rev.*, 41(1):85–101, 1999.

[13] C. Clason and M. V. Klibanov. The quasi-reversibility method for thermoacoustic tomography in a heterogeneous medium. *SIAM J. Sci. Comput.*, 30(1):1–23, 2007/08.

[14] J. E. Dennis and R. B. Schnabel. *Numerical Methods for Unconstrained Optimization and Nonlinear Equations*. SIAM, Philadelphia, PA, 1996.

[15] R. Fletcher. *Practical Methods of Optimization*. John Wiley & Sons, New York, 1987.

[16] P. R. Garabedian. *Partial Differential Equations*. John Wiley & Sons, New York, 1964.

[17] P. E. Gill, W. Murray, and M. H. Wright. *Practical Optimization*. Academic Press, New York, 1981.

[18] Y. A. Gryazin, M. V. Klibanov, and T. R. Lucas. Numerical solution of a subsurface imaging problem. *SIAM J. Appl. Math.*, 62:664–683, 2001.

[19] J. Hadamard. *Lectures on Cauchy's Problem in Linear Partial Differential Equations*. Dover Publications, New York, NY, 1953.

[20] L. Ji and J. R. McLaughlin. Recovery of the Lamé parameter μ in biological tissues. *Inverse Problems*, 20(1):1–24, 2004.

[21] S. I. Kabanikhin, A. D. Satybaev, and M. A. Shishlenin. *Direct Methods of Solving Multidimensional Inverse Hyperbolic Problems*. VSP, Utrecht, 2005.

[22] M. Kac. Can one hear the shape of a drum? *Amer. Math. Monthly*, 73(4):1–23, 1966.

[23] C. T. Kelley. *Iterative Methods for Optimization*. SIAM, Philadelphia, PA, 1999.

[24] M. V. Klibanov. Inverse problems in the 'large' and Carleman bounds. *Diff. Equations*, 20:755–760, 1984.

[25] M. V. Klibanov and F. Santosa. A computational quasi-reversibility method for Cauchy problems for Laplace's equation. *SIAM J. Appl. Math.*, 51(6):1653–1675, 1991.

[26] M. V. Klibanov and A. Timonov. A sequential minimization algorithm based on the convexification approach. *Inverse Problems*, 19:331–354, 2003.

[27] M. V. Klibanov and A. Timonov. *Carleman Estimates for Coefficient Inverse Problems and Numerical Applications*. VSP, Utrecht, The Netherlands, 2004.

[28] M. V. Klibanov and A. Timonov. A unified framework for constructing of globally convergent numerical algorithms for multidimensional coefficient inverse problems. *Applicable Analysis*, 83:933–955, 2004.

[29] L. Landweber. An iteration formula for Fredholm integral equations of the first kind. *Amer. J. Math.*, 73:615–624, 1951.

[30] R. Lattès and J. L. Lions. *The Method of Quasi-reversibility*. American Elsevier, New York, 1969.

[31] J. R. McLaughlin and D. Renzi. Shear wave speed recovery in transient elastography and supersonic imaging using propagating fronts. *Inverse Problems*, 22(2):681–706, 2006.

[32] J. M. Ortega and W. C. Rheinboldt. *Iterative Solution of Nonlinear Equations in Several Variables*. Academic Press, New York, 1970.

[33] L. E. Payne. *Improperly Posed Problems in Partial Differential Equations*. Society for Industrial and Applied Mathematics, Philadelphia, PA, 1975.

[34] E. Polak. *Optimization: Algorithms and Consistent Approximations*. Springer-Verlag, New York, 1997.

[35] H. Shan, M. V. Klibanov, H. Liu, N. Pantong, and J. Su. Numerical implementation of the convexification algorithm for an optical diffusion tomograph. *Inverse Problems*, 24(2):025006, 18pp, 2008.

[36] H. Shan, M. V. Klibanov, J. Su, N. Pantong, and H. Liu. A globally accelerated numerical method for optical tomography with continuous wave source. *J. Inverse Ill-Posed Probl.*, 16(8):763–790, 2008.

[37] J. Su, H. Shan, H. Liu, and M. V. Klibanov. Reconstruction method with data from a multiple-site continuous-wave source for three-dimensional optical tomography. *J. Opt. Soc. Am.*, 23:2388–2395, 2006.

[38] A. N. Tikhonov. On stability of inverse problems. *Dokl. Akad. Nauk SSSR*, 39(5):195–198, 1963.

[39] A. N. Tikhonov. On the solution of ill-posed problems and the method of regularization. *Dokl. Akad. Nauk SSSR*, 151(3):501–504, 1963.

[40] A. N. Tikhonov and V. Y. Arsenin. *Solutions of Ill-Posed Problems*. Winston & Sons., Washington, D.C., 1977.

[41] J. Xin. Comparative study of the least squares approximation of the modified Bessel function. *Comm. Numer. Methods Engrg.*, 24(8):627–633, 2008.

[42] J. Xin and J. E. Flaherty. Viscous stabilization of discontinuous Galerkin solutions of hyperbolic conservation laws. *Appl. Numer. Math.*, 56(3-4):444–458, 2006.

[43] J. Xin and M. V. Klibanov. Comparative studies of the globally convergent convexification algorithm with application to imaging of antipersonnel land mines. *Appl. Anal.*, 86(9):1147–1176, 2007.

[44] J. Xin and M. V. Klibanov. Imaging of land mines by the globally convergent convexification method using a simplified mathematical model. *Inverse Probl. Sci. Eng.*, 16(5):631–653, 2008.

[45] J. Xin and M. V. Klibanov. Numerical solution of an inverse problem of imaging of antipersonnel land mines by the globally convergent convexification algorithm. *SIAM J. Sci. Comput.*, 30(6):3170–3196, 2008.

[46] J. Xin and M. V. Klibanov. High speed imaging of antipersonnel land mines by the convexification algorithm for a simplified mathematical model in two dimensions. *J. Inverse Ill-Posed Probl.*, 17(2):187–207, 2009.